AUTONOMOUS URBAN REGION REPRESENTATION WITH LLM-INFORMED REINFORCEMENT LEARNING

Anonymous authors
Paper under double-blind review

ABSTRACT

Urban representation learning has become a key approach for many applications in urban computing, but existing methods still rely heavily on manual feature designs and geographic heuristics. We present SubUrban, a reinforcement learning framework that autonomously discovers informative regional features through submodular rewards and semantic guidance from large language models. SubUrban adaptively expands each region into a hypernode, suppressing redundancy while preserving complementary associations, and learns cross-task embeddings with a graph-attention policy. Experiments across multiple prediction tasks (population, house price, and GDP) and cities (Beijing, Shanghai, New York, and Singapore) show that SubUrban consistently outperforms state-of-the-art baselines, achieving comparable accuracy with only 10% of the training data. These results highlight submodular-driven automation, enhanced by LLM-in-the-loop semantics, as a practical paradigm for autonomous urban region representation learning. The implementation of our SubUrban is available at https://anonymous.4open.science/r/SubUrban_ICLR2026.

1 Introduction

Over the past decade, the rapid growth of large-scale urban data sources, including remote sensing imagery, points of interest (POIs), and human mobility records, has profoundly reshaped urban computing. These data provide unprecedented opportunities for *urban computing*, enabling applications in social analysis (Meyer & Turner, 1992), economic growth prediction (Hui et al., 2020), air quality modeling (Zheng et al., 2013), and traffic forecasting (Keller et al., 2020). Despite these advances, many approaches are tailored to specific tasks (Shimizu et al., 2021; Pulugurtha et al., 2013; Naik et al., 2014), require extensive labels, and cannot be readily adapted to other tasks.

Urban region representation learning (also called *urban region embedding*) has emerged as a promising approach to produce universal feature vectors of city regions that can be reused across tasks. The intuition is that urban applications often rely on common geospatial features. For instance, Wang et al. (Wang & Li, 2017) show that human mobility strongly correlates with socio-economic indicators such as crime rates, house prices, and household income. By embedding taxi trajectories into region representations, they achieved accurate predictions across diverse tasks. Building on this idea, subsequent studies generally combine two complementary perspectives: intra-region semantics and inter-region associations. Intra-region semantics characterize what is inside a region, such as building density, POI types, or land-use composition (Yuan et al., 2012; Zhang et al., 2017b; Yao et al., 2018; Fu et al., 2019; Zhang et al., 2020; Wang et al., 2020; Xi et al., 2022; Li et al., 2023; Huang et al., 2023; Balsebre et al., 2024). Inter-region associations describe how regions are related, for instance, through spatial proximity, functional similarity, or traffic connectivity (Wang & Li, 2017; Yao et al., 2018; Fu et al., 2019; Zhang et al., 2019; 2020; Wu et al., 2022; Zhang et al., 2022). These approaches reduce the cost of designing and training task-specific models.

Nevertheless, existing methods still demand significant human effort. For intra-region semantics, contrastive learning is widely used to highlight informative samples while suppressing noise, but it depends heavily on handcrafted geographic heuristics. For example, HGI (Huang et al., 2023) treats regions with moderately similar embeddings (cosine similarity 0.6–0.8) as hard negatives, while

RegionDCL (Li et al., 2023) selects regions with similar building clusters as positives to capture functional correlations. Such heuristics require domain expertise and suffer from costly preprocessing and training. For inter-region associations, researchers typically construct urban graphs where nodes represent POIs, buildings, or areas, and edges are derived from spatial distance, trajectories, or feature similarity. This giant design space makes it unclear which relations are most useful, often requiring extensive city-specific tuning and ad-hoc feature engineering. These challenges raise a central research question: Can we design a framework that automatically identifies the most informative intra- and inter-region features to learn region embeddings, without relying on manual heuristics or city-specific adjustments?

In this work, we identify two key challenges for automated region representation learning. First, prioritizing informative intra-region features requires domain knowledge, since not all input features are informative for downstream tasks, and real-world datasets often contain substantial redundancy and noise. For example, real-world POI datasets often contain large fractions of duplicated or low-informative entries such as addresses, phone numbers, or building facilities (e.g., block numbers, floor indices, elevators). Simply aggregating such entries not only increases computational overhead but also degrades the quality of learned embeddings. Second, the vast design space of graph structures makes it difficult to extract meaningful inter-region associations. Searching over possible urban graph constructions is both computationally expensive and challenging to optimize, as the number of candidate edges grows quadratically with the number of graph nodes.

To address these challenges, we propose **SubUrban**, a submodular-driven reinforcement learning framework for autonomous urban representation learning. SubUrban leverages submodular functions to suppress redundant POIs and prioritize informative features, while large language models provide city-specific heuristics to filter low-value data and highlight representative urban landmarks, enabling semantic-aware intra-region modeling. For inter-region relations, SubUrban applies submodular hypernode expansions that progressively connect each region to nearby and semantically complementary areas. This approach prunes the quadratic growth of candidate edges by retaining associations with the highest marginal utility. Experiments across multiple cities and tasks show that SubUrban outperforms state-of-the-art baselines with only 10% of the data, confirming the effectiveness of its redundancy suppression and semantic-aware selection strategies. To summarize, our contributions are at least threefold:

- We propose a novel <u>Sub</u>modular-driven reinforcement learning paradigm for autonomous <u>Urban</u> representation learning, eliminating the need for manual feature engineering and heuristic designs in data selection and region modeling.
- We introduce an LLM-informed framework that provides urban expertise and semantic guidance for informative candidate selection and exploration acceleration, enhancing both convergence efficiency and cross-city transferability.
- Extensive experiments demonstrate that SubUrban consistently outperforms state-of-the-art baselines across multiple tasks and cities, while achieving up to 90% data efficiency and robust transferability under diverse urban areas.

2 Related Work

Urban Region Representation Learning Early studies relied on task-specific features such as mobility patterns, social media check-ins, or remote sensing imagery for applications including air quality modeling, functional zone identification, and urban safety analysis (Yuan et al., 2012; Zheng et al., 2013; Yao et al., 2018; Naik et al., 2014). More recent work has shifted toward self-supervised paradigms that capture spatial correlations or inter-region interactions. Examples include flow-based embedding models (Wang & Li, 2017; Fu et al., 2019), proximity-constrained or contrastive approaches with graph encoders (Zhang et al., 2019; 2022), and multimodal fusion of text, imagery, and mobility signals (Jenkins et al., 2019; Zhang et al., 2017a; 2020; Wu et al., 2022). Extensions further incorporate heterogeneous data such as satellite imagery and building footprints (Li et al., 2023; Huang et al., 2023; Balsebre et al., 2024; Yan et al., 2024; Wang et al., 2020). While these methods significantly improve reusability across tasks, they still depend on heuristic choices for sample construction and city-specific tuning, and often suffer from redundancy when large-scale urban data are indiscriminately included.

LLMs for Urban Tasks Large Language Models (LLMs) have recently been applied to urban computing for their ability to enrich semantics and contextual reasoning. Representative directions include domain adaptation for geoscientific corpora (Deng et al., 2024), LLM-guided region descriptions (Fu et al., 2024), and LLM-agent frameworks for building urban knowledge graphs and aligning heterogeneous sources (Ning & Liu, 2024; Manvi et al., 2024). These works highlight the potential of LLMs in urban data mining, but their role in guiding representation learning remains underexplored, particularly in evaluating and prioritizing informative regional features.

3 PRELIMINARIES

Definition 1 (Urban Hypernode). An urban hypernode S_r is an extended representation unit that includes both POIs within a region r and selected POIs from its δ -neighborhood. Given candidates $\mathcal{P}_r = \{p \in POI \mid dist(p,r) \leq \delta\}$, a subset $S_r \subseteq \mathcal{P}_r$ is chosen based on spatial structure, semantic relevance, and submodular rewards. The resulting hypernode (r, S_r) enriches region representation with contextual information beyond the boundary.

Definition 2 (Urban Region Representation Learning). Given regions $\mathcal{U} = \{u_1, \dots\}$, the goal is to learn a mapping that produces a vector $\mathbf{z}_i \in \mathbb{R}^d$ for each $u_i \in \mathcal{U}$, which can be used in downstream prediction tasks such as population density or housing price prediction.

Definition 3 (Submodular Reinforcement Learning). Submodular reinforcement learning models rewards as submodular set functions to capture diminishing returns. For a ground set V, a function $F: 2^V \to \mathbb{R}$ is submodular if

$$F(A \cup \{v\}) - F(A) \ge F(B \cup \{v\}) - F(B)$$
 (1)

for all $A \subseteq B \subseteq V$ *and* $v \in V \setminus B$.

Problem Statement. Given a set of urban regions $\mathcal{R} = \{r_1, \dots, r_n\}$ with their surrounding POI distributions, our goal is to learn an adaptive expansion policy network that constructs urban hypernodes for optimal region representation. Formally, we aim to optimize:

$$\pi_{\theta}^* = \arg \max_{\pi_{\theta}} \mathbb{E}_{r \sim \mathcal{R}} \left[R \left((r, \pi_{\theta}(\mathcal{P}_r)), \mathcal{T} \right) \right]$$
 (2)

where $\pi_{\theta}: \mathcal{P}_r \to \mathcal{S}_r \subseteq \mathcal{P}_r$ represents the expansion policy network that selects POI subset \mathcal{S}_r from the candidate set \mathcal{P}_r , and $R(\cdot, \mathcal{T})$ denotes the reward function evaluated on downstream tasks \mathcal{T} . It is noteworthy that we focus on POIs in this work since they are the most widely used features in literature (Chen et al., 2024); however, the framework is general and can be extended to other textual inputs or adapted to visual modalities via vision–language models.

4 METHODOLOGY

We present the SubUrban framework, which comprises three key components as illustrated in Figure 1: (1) **POI Set Preprocessing** applies LLM-guided semantic retrieval and spatial clustering to condense raw POI data while preserving structural diversity and functional relevance. (2) **Submodular-Aware Reinforcement Learning** formulates POI selection as a sequential decision task, where an agent selects POIs based on submodular utility within structured spatial contexts. (3) **LLM-Instructed CEM Optimization** calibrates attention weights of POI categories based on heuristics from LLM instruction to enhance semantic alignment and accelerate convergence.

4.1 POI SET PREPROCESSING

Urban data such as POIs, check-ins, and geo-tagged tweets are often massive, noisy, and redundant. Existing approaches either manually curate a limited set of useful inputs, which requires significant human labor and domain knowledge, or simply feed all available data into training, which increases computation and amplifies noise. To address these problems, we adopt a more selective strategy with LLMs. Instead of feeding all candidate POI to LLMs, which would be prohibitively costly and slow, we only provide the administrative region's name and address, prompting it to generate heuristic keywords. For well-known regions, the model tends to return landmarks and attractions (e.g., Times Square), while for less prominent regions it generates important functional roles (e.g., residential

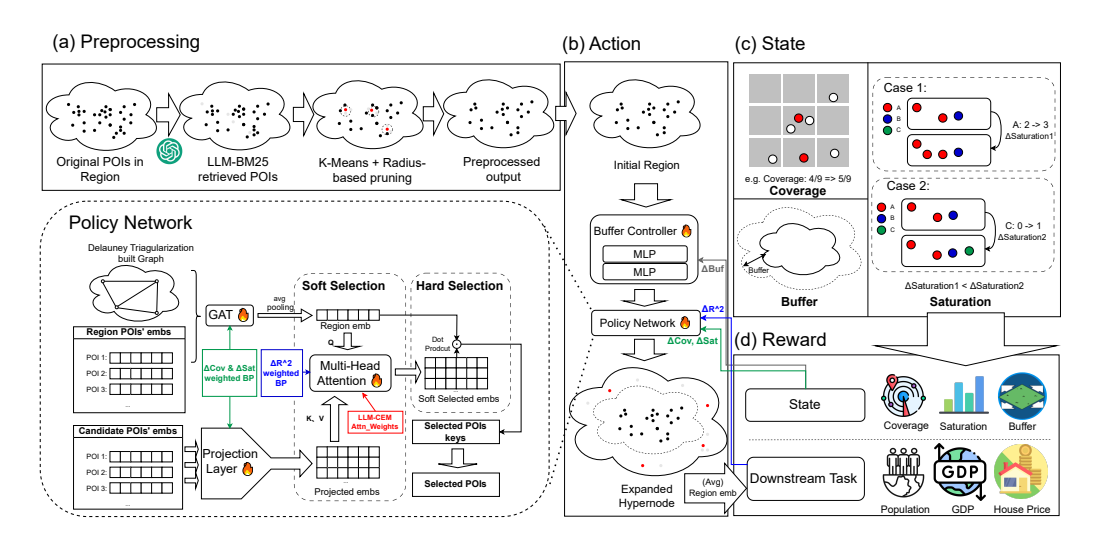


Figure 1: Overview of the SubUrban learning framework. With a defined triplet (Coverage, Saturation, Buffer) as the State, delta values of mixed downstream results and states as Reward, a two-stage policy network as Action to extend POI.

or industrial) of the area. We then apply off-the-shelf retrieval methods (e.g., BM25 (Robertson & Walker, 1994)) to locate POIs that match these keywords. Next, K-means clustering is applied to regulate spatial density and ensure more uniform coverage across the regions, resulting in a functionally representative subset of POIs, which can serve as reliable starting points for further expansion.

4.2 Submodular-Aware Reinforcement Learning

To automate the process of identifying informative intra- and inter-region features, we mimic how human experts gradually refine their understanding of a city. Rather than fixing rules in advance, experts iteratively select features, evaluate their usefulness based on domain-specific criteria or validation tasks, and adjust their choices accordingly. This adaptive trial-and-error process is naturally aligned with reinforcement learning, formalized by a three-tuple (state, action, reward). In our setting, these are defined as geospatial states, feature-selection actions, and submodular-aware rewards.

4.2.1 GEOSPATIAL-DEFINED STATE

We define the **state** to capture the properties of currently selected POIs, summarizing their spatial extent (**Coverage, Cov**), semantic diversity (**Saturation, Sat**), and potential for future expansion (**Buffer, Buf**). Intuitively, each POI represents certain urban functions within its surrounding area¹. The buffer component (**Buf**) is inspired by previous submodular RL work (Prajapat et al., 2024), reflecting the fact that adding more data points beyond a certain level brings diminishing returns. Once key urban functions are sufficiently represented, further expansion offers little additional benefit.

Formally, we represent the state as a triplet $State_t = (Cov_t, Sat_t, Buf_t)$, where

$$Cov_t = \frac{|\{g : g \cap S_t \neq \emptyset\}|}{|\mathcal{G}|}, \quad Sat_t = -\frac{1}{\log C} \sum_c q_c \log q_c, \quad Buf_t = f_{\mathsf{MLP}}(\mathsf{State}_{t-1}). \tag{3}$$

Here, Cov_t denotes the proportion of grid cells already covered by selected POIs from the current selection set S_t , where $\{g:g\cap S_t\neq\emptyset\}$ represents the set of grid cells that intersect with at least one POI in Sat_t . Sat_t is the normalized entropy of POI categories that reflects semantic diversity. Buf_t is an adaptive expansion radius predicted by a two-layer MLP with softplus activation to control how far new candidates are retrieved at step t.

¹The intuition is general and can be adapted to other urban data types like buildings and street-view images.

4.2.2 GEOSPATIAL-BASED ACTION

In the SubUrban framework, the action represents how the system autonomously expands the regional POI set to construct more informative hypernodes. Because neither human experts nor LLMs can exhaustively examine city-scale data, we mimic the strategy of human experts who first conduct fine-grained sensing to capture potentially useful information, and then apply a unified standard to filter the data. Following this intuition, our policy alternates between soft selection, which preserves recall through attention-based scoring of candidate POIs, and hard selection, which contracts the set by dot-product similarity to produce a compact and representative subset.

Soft Selection We assess the importance of candidate POIs by evaluating how their features contribute to the aggregated region embeddings. We encode intra-region POIs with a Graph Attention Network (GAT) using Delaunay triangulation (Delaunay, 1934) edges \mathcal{E}_r following Huang et al. (2023); Balsebre et al. (2024); Li et al. (2023), and apply average pooling to obtain the region embedding \mathbf{z}_r . Then, each candidate \mathbf{p}_i is projected into the same dimension via W_p , and its importance score α is estimated by averaging attention scores from H attention heads:

$$\mathbf{z}_r = \frac{1}{|S_r|} \sum_{j \in S_r} \text{GAT}(\mathbf{p}_j, \mathcal{E}_r), \quad \alpha_i = \frac{1}{H} \sum_{h=1}^H \text{Attn}(\mathbf{z}_r, W_P \mathbf{p}_i).$$
 (4)

The scores are then reweighted by category weights $w_{c(i)}$ from the LLM-instructed CEM process in Section 4.3, and candidates and their associated edges are retained only if their weighted scores exceed the threshold, with an additional cap of $K_{\rm soft}$ to prevent oversampling in dense regions.

$$\tilde{\alpha}_i = \alpha_i \cdot w_{c(i)}, \quad \bar{\tilde{\alpha}} = \frac{1}{|\mathcal{B}_r|} \sum_{j \in \mathcal{B}_r} \tilde{\alpha}_j, \quad \mathcal{S}_r^{\text{soft}} = \text{Top}_{K_{\text{soft}}} \{ \mathbf{p}_i \in \mathcal{B}_r \mid \tilde{\alpha}_i \ge \bar{\tilde{\alpha}} \}.$$
 (5)

Hard Selection To obtain a compact and consistent subset, we refine the soft candidates by dot-product similarity to the regional embedding \mathbf{z}_r . Each similarity score is reweighted by the same category preferences and compared against the mean score $\bar{\mathbf{s}}$. Only candidates above this threshold are retained, subject to a cap K that prevents oversampling in dense regions:

$$\mathcal{S}_r^{(t)} = \left\{ \mathbf{p}_i \in \mathcal{S}_r^{\text{soft}} \mid w_{c(i)} \cdot (\mathbf{z}_r^\top W_P \mathbf{p}_i) \ge \bar{\mathbf{s}}, \ |\mathcal{S}_r^{(t)}| \le K \right\}.$$
 (6)

Here $\bar{\mathbf{s}}$ denotes the mean of all weighted similarity scores within $\mathcal{S}_r^{\text{soft}}$. This step contracts the candidate pool into a smaller yet representative subset, and we set $K_{\text{soft}} = 1.5K$ for simplicity.

The soft and hard selections are executed alternately, removing redundant POIs and edges while preserving informative ones. With the guidance of the reward signals, it progressively shapes more coherent submodule structures across regions, thereby capturing useful inter-region relationships.

4.2.3 REWARD AND LOSS FUNCTIONS

Reward Function Different modules in SubUrban focus on different aspects of the learning process, so we design tailored reward signals rather than a single global metric. Intuitively, the GAT and projection layers should capture local improvements in spatial coverage and semantic diversity, the attention module should be aware of the global task performance, and the buffer controller should balances task performance with expansion constraints. We define three reward signals corresponding to the GAT, Projection Layer, Multhead Attention, and buffer controller modules:

$$R_{\rm GAT} = R_{\rm proj} = \frac{\Delta_{\rm sat}}{\sigma_{\rm sat}} + \frac{\Delta_{\rm cov}}{\sigma_{\rm cov}},\tag{7}$$

$$R_{\rm MHA} = \frac{\Delta_{\rm downstream}}{\sigma_{\rm downstream}},\tag{8}$$

$$R_{\rm buf} = \frac{\Delta_{\rm downstream}}{\sigma_{\rm downstream}} + \alpha_{\rm buf} \cdot \frac{\Delta_{\rm buf}}{\sigma_{\rm buf}} - \max(\Delta_{\rm buf} - \beta_{\rm buf} \cdot \operatorname{Buf}_t, 0) \,. \tag{9}$$
Here $R_{\rm GAT}$ and $R_{\rm proj}$ guide the GAT and Projection Layer using local state signals, i.e., improve-

Here $R_{\rm GAT}$ and $R_{\rm proj}$ guide the GAT and Projection Layer using local state signals, i.e., improvements in semantic diversity ($\Delta_{\rm sat}$) and spatial coverage ($\Delta_{\rm cov}$). $R_{\rm MHA}$ directs the Multihead Attention using improvements in downstream task performance on the validation set ($\Delta_{\rm downstream}$). $R_{\rm buf}$ steers the buffer controller by combining downstream performance with expansion constraints, controlled by $\alpha_{\rm buf}$ and $\beta_{\rm buf}$ (with sensitivity analyzed in Appendix D.4). All reward terms are normalized by historical standard deviations ($\sigma_{\rm sat}$, $\sigma_{\rm cov}$, $\sigma_{\rm downstream}$, $\sigma_{\rm buf}$) to stabilize scales without manual tuning.

Advantage Function. To reduce reward variance and stabilize training across modules, each module maintains an Exponential Moving Average (EMA) that tracks the expected reward over time. The advantage function for continuous-time reinforcement learning (Baird, 1994) is applied to compute the difference between the current reward and EMA, providing a normalized signal that indicates whether the current performance exceeds historical expectations:

$$A_{t}^{(m)} = R_{t}^{(m)} - b_{t}^{(m)}, \quad b_{t}^{(m)} = \gamma_{t} \cdot b_{t-1}^{(m)} + (1 - \gamma_{t}) \cdot R_{t}^{(m)}, \quad \gamma_{t} = \sigma \left(\frac{\|R_{t-1}^{(m)} - R_{t-2}^{(m)}\|}{\|R_{t-1}^{(m)}\| + \epsilon} \right)$$
(10)

where (m) can be modules including GAT, Projection Layer, Multihead Attention, and Buffer Controller. And γ_t is the adaptive EMA coefficient computed from reward variability when sufficient training history becomes available, eliminating manual parameter tuning.

Loss and Gradient Updates Each module employs advantage-weighted gradient updates with distinct optimization strategies tailored to its specific learning objectives. The Buffer Controller uses PPO-style clipped ratios for stability, the Multihead Attention mechanism applies cross-entropy loss weighted by mixed-task advantages to optimize selection quality, while GAT and Projection Layer directly use advantage-weighted updates to optimize state representation quality:

$$\nabla_{\theta_{\text{buf}}} \mathcal{L}_{\text{buf}} = -\mathbb{E}\left[\min(r_t A_t^{\text{buf}}, \text{clip}(r_t, 1 - \epsilon, 1 + \epsilon) A_t^{\text{buf}})\right]$$
(11)

$$\nabla_{\theta_{\text{MHA}}} \mathcal{L}_{\text{MHA}} = -\mathbb{E}\left[\mathcal{L}_{\text{cross-entropy}} \cdot A_t^{\text{MHA}}\right]$$
 (12)

$$\nabla_{\theta_{\text{GAT,proj}}} \mathcal{L}_{\text{GAT,proj}} = -\mathbb{E}\left[A_t^{\text{GAT,proj}}\right]$$
(13)

where r_t is the ratio of action probabilities under the updated and previous buffer policies following PPO settings (Schulman et al., 2017).

4.3 LLM-Instructed CEM Optimization

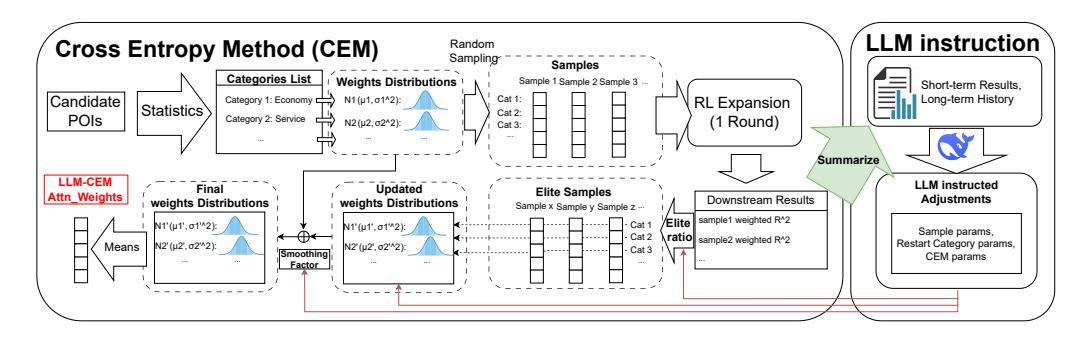


Figure 2: LLM-instructed CEM tunes category weights of POIs in the Multihead Attention module from the policy network.

Human-designed heuristics have proven effective in previous studies Chen et al. (2024), but they demand costly manual effort. In SubUrban, we instead use a Large Language Model to inject heuristics automatically. The LLM can continuously observe the evolving optimization process, improving the selection and accelerating the convergence via its feedback. Specifically, we initialize the category weights $\{w_c\}_{c=1}^C$ that scale the attention scores in Eq. 5 via Cross Entropy Method (CEM), which iteratively samples candidate weight vectors from Gaussian distributions with per-category means $\mu_c^{(t)}$ and standard deviations $\sigma_c^{(t)}$, selects "elite samples" based on downstream task performance, and updates the distribution toward samples with high performance as follows:

$$\mu_c^{(t+1)} = \alpha \,\mu_c^{(t)} + (1 - \alpha) \,(\mu_{\text{elite}}^{(t)})_c, \quad \sigma_c^{(t+1)} = \alpha \,\sigma_c^{(t)} + (1 - \alpha) \,(\sigma_{\text{elite}}^{(t)})_c \tag{14}$$

Then, we utilize the Large Language Model to analyze optimization behavior and provide targeted parameter adjustments. The LLM observes both recent optimization behavior and long-term history, and proposes heuristic adjustments to distribution parameters and stability factors. This high-level guidance complements the sampling-driven updates of CEM, while detailed interaction protocols and implementation settings are deferred to Appendix C.2 and Appendix B.

5 EXPERIMENTS

In this section, we evaluate the proposed method and the derived representation of extended POI subsets following previous literature (Li et al., 2023; Balsebre et al., 2024). We also perform ablation studies, case studies, and parameter sensitivity analysis.

5.1 EXPERIMENTAL SETTINGS

Dataset We conduct experiments using inputs of POI datasets collected via the Gaode Map API for Beijing and Shanghai, while from OSM for Singapore and New York City. The statistics of POI datasets are shown in Table 1.

Table 1: Dataset Statistics

City	POIs	POI categories	Regions
Beijing	1,218,188	23	1,253
Shanghai	1,192,123	22	1,688
Singapore	269,961	759	2,520
New York City	283,810	65	2,280

Baselines and Metrics We compare SubUrban against seven urban region representation

learning baselines through POI encoding: BERT (Devlin et al., 2019a), OpenAI (Neelakantan et al., 2022), GraphSage (Hamilton et al., 2017), DGI (Zhao et al., 2023), MVGRL (Hassani & Ahmadi, 2020), HGI (Huang et al., 2023), and CityFM (Balsebre et al., 2024), with details in Appendix D.1. We focus on POI encoding methods since our approach addresses diminishing returns from POI data specifically. Evaluation is conducted on three regression tasks: population density prediction, house price prediction, and GDP density prediction using the classifier of Random Forest with 4:1 train/test splits. We report the performance through average and standard deviation across 5 runs with different random seeds under 5-fold cross-validation, using Mean Absolute Error (MAE), Root Mean Squared Error (RMSE), and Coefficient of Determination (R²) metrics.

5.2 EXPERIMENTAL RESULTS

We evaluate the quality of derived representations from our proposed SubUrban and other baselines from cross-city and cross-task aspects.

5.2.1 Cross-City Performance

Table 2: Population Density Prediction in Beijing, Shanghai, Singapore, and NYC

Models	Beijing			Shanghai		Singapore			NYC			
	MAE↓	RMSE↓	$R^2\uparrow$	MAE↓	RMSE↓	$R^2\uparrow$	MAE↓	RMSE↓	$R^2\uparrow$	MAE↓	RMSE↓	$R^2\uparrow$
BERT-Avg	5043.73 (±170.77)	8203.42) (±198.00)	0.49 (±0.02)	9375.19 (±75.37)	14235.93 (±203.54)	0.47 (±0.01)	4.11 (±0.20)	5.97 (±0.27)	0.68 (±0.03)	5325.16 (±129.20)	6845.95 (±159.71)	0.56 (±0.02)
OpenAI-Avg	5419.69 (±158.87)	8440.61 (±172.59)	$0.46 \\ (\pm 0.02)$	9816.80 (±108.09)	14579.09 (±305.37)	0.44 (±0.02)	4.01 (±0.16)	5.89 (±0.17)	0.69 (±0.03)	3858.68 (±102.36)	5366.48 (±201.16)	0.73 (±0.02)
GraphSage	4774.99 (±269.06)	7812.94 (±578.01)	$0.52 \ (\pm 0.07)$	8759.62 (±388.16)	13682.10 (±644.79)	0.53 (± 0.02)	3.44 (±0.19)	5.16 (±0.41)	$0.76 \\ (\pm 0.02)$	4025.13 (±95.00)	5502.47 (±140.00)	0.72 (± 0.02)
DGI			` ,	,	14110.26 (±1157.06)	. ,	. ,	. ,	. ,	(5847.58 (±110.30)	0.69 (± 0.01)
MVGRL	(<u> </u>	, (—- ,	((,	13646.88 (± 1078.60)	((((6414.38 (± 115.52)	(
HGI					11642.35 (± 289.60)	. ,	. ,	5.27 (±0.14)	. ,	. ,	5424.56 (± 158.39)	. ,
CityFM	$\frac{4199.19}{(\pm 65.02)}$	$\frac{6858.44}{(\pm 143.30)}$	(± 0.02)	$\frac{6558.20}{(\pm 108.37)}$	$\frac{10677.55}{(\pm 218.36)}$	(± 0.01)	(± 0.09)	$\frac{3.89}{(\pm 0.25)}$	(± 0.01)	$\frac{3697.40}{(\pm 122.25)}$	$\frac{5243.60}{(\pm 196.12)}$	(± 0.02)
SubUrban	3283.11 (±273.61)	5719.89 (±640.22)	0.72 (±0.06)	5684.80 (±356.93)	9673.78 (±716.99)	0.75 (±0.02)	1.84 (±0.04)	2.85 (±0.11)	0.85 (±0.01)	3401.17 (±167.26)	4937.25 (±245.88)	0.77 (±0.02)

We conduct population density prediction experiments across four diverse cities (Beijing, Shanghai, Singapore, and New York City) to evaluate the cross-city adaptability of SubUrban. Table 2 shows that graph structural methods (GraphSAGE, DGI, MVGRL) exhibit inconsistent performance among different cities, suggesting that differences in urban planning contexts affect the effectiveness of graph learning. Strong baselines incorporating both semantic and spatial contexts (HGI, CityFM)

Table 3: Population Density, House Price, and GDP Density Prediction in Beijing

Models	Population			House Price			GDP Density		
	MAE↓	RMSE↓	$R^2\uparrow$	MAE↓	RMSE↓	$R^2\uparrow$	MAE↓	RMSE↓	$R^2\uparrow$
DEDT A	5043.73	8203.42	0.49	14391.39	20622.46	0.74	490.47	789.56	0.62
BERT-Avg	(± 170.77)	(± 198.00)	(± 0.02)	(± 681.11)	(± 785.23)	(± 0.03)	(± 36.14)	(± 62.61)	(± 0.04)
Oman A.I. Avia	5419.69	8440.61	0.46	13946.38	20105.17	0.75	523.66	815.47	0.59
OpenAI-Avg	(± 158.87)	(± 172.59)	(± 0.02)	(± 695.83)	(± 1155.70)	(± 0.03)	(± 42.84)	(± 67.57)	(± 0.03)
CuambCasa	4774.99	7812.94	0.52	14748.74	22275.26	0.69	488.91	782.01	0.63
GraphSage	(± 269.06)	(± 578.01)	(± 0.07)	(± 2750.97)	(± 5175.66)	(± 0.17)	(± 36.89)	(± 89.28)	(± 0.04)
DCI	4990.86	8153.15	0.47	15357.90	20122.38	0.75	466.77	743.05	0.67
DGI	(± 150.99)	(± 522.52)	(± 0.07)	(± 1876.32)	(± 3558.96)	(± 0.06)	(± 23.28)	(± 74.46)	(± 0.05)
MVGRL	4990.86	8153.15	0.47	15692.40	22317.73	0.70	502.90	840.42	0.57
MVGKL	(± 150.99)	(± 522.52)	(± 0.07)	(± 1534.83)	(± 3920.51)	(± 0.04)	(± 25.72)	(± 69.60)	(± 0.07)
HGI	4534.83	7446.83	0.56	14719.13	19008.63	0.78	409.07	695.99	0.70
поі	(± 473.15)	(± 746.63)	(± 0.09)	(± 1378.46)	(± 1834.69)	(± 0.05)	(± 34.54)	(± 69.44)	(± 0.02)
CityFM	4199.19	6858.44	0.64	14291.54	19483.32	0.75	384.27	601.26	0.78
Спугм	(± 65.02)	(± 143.30)	(± 0.02)	(± 371.40)	(± 582.32)	(± 0.02)	(± 18.37)	(± 48.58)	(± 0.04)
SubUrban	3283.11 (±273.61)	5719.89 (±640.22)	0.72 (±0.06)	12235.97 (±1249.12)	17021.29 (±2364.06)	0.85 (±0.03)	349.63 (±27.50)	568.85 (±42.24)	0.80 (±0.03)

acl

achieve more consistent results across cities, with CityFM demonstrating the best baseline performance through extensive OpenStreetMap pretraining. SubUrban outperforms all baselines across all four cities, demonstrating cross-city adaptability using only 10% of the full POI set.

5.2.2 Cross-Task Performance

We extend the evaluation to house price and GDP density prediction in Beijing to evaluate the cross-task adaptability of SubUrban. Table 3 shows that graph structural methods (GraphSAGE, DGI, MVGRL) exhibit inconsistent performance across cities and tasks, often comparable to simple averaging (BERT-Avg). These methods show better performance in Singapore and NYC compared to Beijing and Shanghai, suggesting urban planning differences affect effectiveness. Strong baselines (HGI, CityFM) demonstrate more consistent results, with CityFM achieving superior population prediction through OpenStreetMap pretraining, while HGI shows stronger house price prediction via rule-based negative sampling. SubUrban consistently outperforms all baselines across all tasks, especially achieving notable improvements in Population Density and House Price prediction tasks, which demonstrates the cross-task adaptivity.

5.2.3 EFFICIENCY ANALYSIS

We compare the Total Processing Time in minutes between our proposed SubUrban and strong baselines (CityFM and HGI). The total processing time includes the time of data preprocessing, model training, and encoding with evaluations. SubUrban achieves the shortest processing time with the highest performance among strong baselines as it utilizes LLMs to efficiently filter out noise POIs and accelerate convergence, while baselines spend much time on training with redundant POIs.

Table 4: Total Processing Time (Minutes)

Method	Beijing	Shanghai
CityFM	535	609
HGI	2262	3790
SubUrban	375	395
Saves (%)	29.9%	35.1%

5.3 ABLATION STUDIES

Impact of Model Components We validate the effect of key components within SubUrban by comparing with the following variants: **w/o RL**: excludes RL-driven expansion, using random expansion instead; **w/o CEM**: omits LLM-instructed CEM optimization; **Ours**: the complete Sub-Urban framework. The results in Figure 3 demonstrate that both components significantly enhance prediction performance across all metrics. The absence of RL leads to the most substantial performance decline, with MAE increasing by approximately 8-12% for population prediction and 4-8% for house price prediction across both cities, confirming that intelligent RL-driven expansion is crucial for capturing optimal spatial patterns. Removing CEM optimization also degrades performance

with consistent drops of 2-4% across all metrics. Additionally, we evaluate the LLM instruction by comparing LLM preprocessed POIs against random sampling and LLM-instructed CEM against pure CEM optimization, finding consistent improvements in training convergence and reward curves (details in Appendix D.3, and more studies in Appendix D.5).

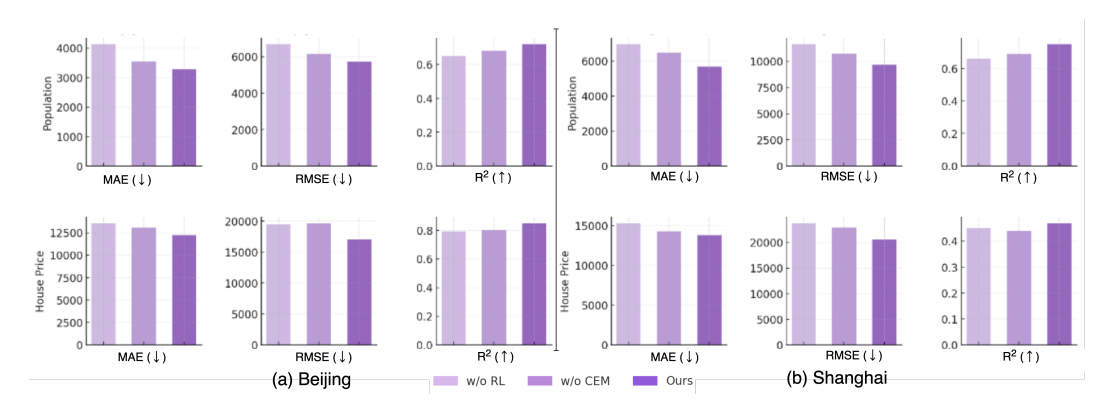


Figure 3: Ablation results of Population Density (first row) and House Price prediction.

Impact of Data-sparsity Since urban data is unevenly distributed in space, we evaluate how Sub-Urban adapts to POI-sparse regions. We partition all regions into four groups of equal size (328 each) based on POI counts and report the MAEs of both tasks in Figure 4. The results show that SubUrban consistently achieves the lowest prediction errors across all density levels, and remains superior to baselines even when using only 10% of the full POI set. This robustness to data sparsity suggests that SubUrban can generalize better across cities with varying information densities.

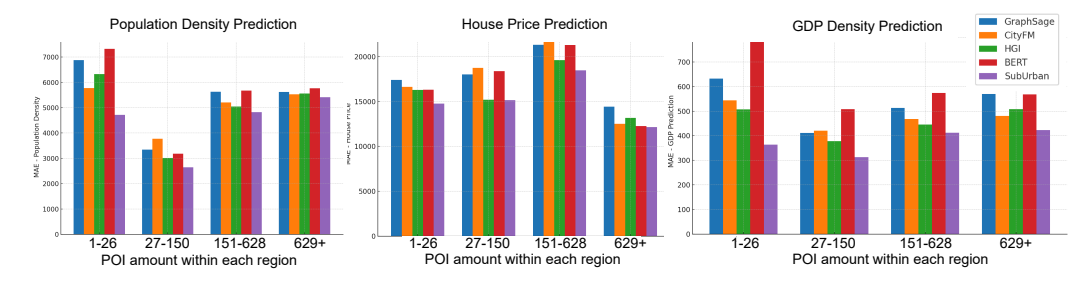


Figure 4: Mean Absolute Error (MAE) of Prediction tasks in regions with different numbers of POIs in Beijing.

Parameter Sensitivity Analysis We further analyze the sensitivity of SubUrban on the penalty coefficient α and the Top-K, where SubUrban achieves stable performance across wide ranges of both parameters, indicating robustness and reducing the need for expert tuning. Due to the page limit, we present the details in Appendix D.4.

6 Conclusion

In this work, we propose SubUrban, a submodular-aware reinforcement learning framework for urban region representation, focusing on automatically identifying POIs that maximize informativeness and adaptivity while minimizing redundancy. By jointly modeling coverage, saturation, and buffer through a hypernode expansion process, SubUrban adaptively prioritizes spatially and semantically complementary POIs while mitigating redundancy from start to convergence, enabling effective selection and efficient optimization under the vast design space. Experiments on cross-city and cross-task comparison demonstrate superior performance over strong baselines with up to 90% less data, robustness across varying POI densities, and insensitivity with respect to buffer distance and candidate set size. This study establishes a new paradigm of autonomous urban representation learning, offering a transformative framework across cities and tasks with improved robustness, transferability, and data efficiency.

ETHICS STATEMENT

We leverage publicly available and non-identifiable data sources, including POI datasets collected from Gaode Map API for Beijing and Shanghai, and OpenStreetMap for Singapore and New York City. All datasets contain only aggregated place-level information without any personal identifiers. No individual-level mobility records or sensitive demographic data are used. Our proposed framework focuses on urban region representation learning with the aim of improving predictive modeling of population density, house prices, and GDP density at the regional level. Our methodology cannot be used to identify or track specific individuals.

REPRODUCIBILITY STATEMENT

We have made careful efforts to ensure the reproducibility of our work. The overall framework design, including the submodular-driven reinforcement learning formulation and the hypernode expansion process, is described in Section 4.2. Implementation settings are reported in Appendix B. Dataset statistics and sources are presented in Table 1 and Table 5. Finally, we will release anonymized source code through the link at the end of the Abstract to facilitate independent verification and reproduction of experiments.

REFERENCES

- L.C. Baird. Reinforcement learning in continuous time: advantage updating. In *Proceedings of 1994 IEEE International Conference on Neural Networks (ICNN'94)*, volume 4, pp. 2448–2453 vol.4, 1994. doi: 10.1109/ICNN.1994.374604.
- Pasquale Balsebre, Weiming Huang, Gao Cong, and Yi Li. City foundation models for learning general purpose representations from openstreetmap. In Edoardo Serra and Francesca Spezzano (eds.), *Proceedings of the 33rd ACM International Conference on Information and Knowledge Management, CIKM 2024, Boise, ID, USA, October 21-25, 2024*, pp. 87–97. ACM, 2024. doi: 10.1145/3627673.3679662.
- Yile Chen, Weiming Huang, Kaiqi Zhao, Yue Jiang, and Gao Cong. Self-supervised learning for geospatial AI: A survey, 2024.
- Boris Delaunay. Sur la sphère vide. a la mémoire de georges voronoï. *Izvestiya Rossiiskoi Akademii Nauk. Seriya Matematicheskaya*, (6):793–800, 1934.
- Cheng Deng, Tianhang Zhang, Zhongmou He, Qiyuan Chen, Yuanyuan Shi, Yi Xu, Luoyi Fu, Weinan Zhang, Xinbing Wang, Chenghu Zhou, Zhouhan Lin, and Junxian He. K2: A foundation language model for geoscience knowledge understanding and utilization, 2024.
- Jacob Devlin, Ming-Wei Chang, Kenton Lee, and Kristina Toutanova. BERT: pre-training of deep bidirectional transformers for language understanding. In Jill Burstein, Christy Doran, and Thamar Solorio (eds.), Proceedings of the 2019 Conference of the North American Chapter of the Association for Computational Linguistics: Human Language Technologies, NAACL-HLT 2019, Minneapolis, MN, USA, June 2-7, 2019, Volume 1 (Long and Short Papers), pp. 4171–4186. Association for Computational Linguistics, 2019a. doi: 10.18653/V1/N19-1423.
- Jacob Devlin, Ming-Wei Chang, Kenton Lee, and Kristina Toutanova. BERT: pre-training of deep bidirectional transformers for language understanding. In Jill Burstein, Christy Doran, and Thamar Solorio (eds.), Proceedings of the 2019 Conference of the North American Chapter of the Association for Computational Linguistics: Human Language Technologies, NAACL-HLT 2019, Minneapolis, MN, USA, June 2-7, 2019, Volume 1 (Long and Short Papers), pp. 4171–4186. Association for Computational Linguistics, 2019b. doi: 10.18653/V1/N19-1423.
- Jiayi Fu, Haoying Han, Xing Su, and Chao Fan. Towards human-ai collaborative urban science research enabled by pre-trained large language models. *Urban Inform.*, 3(1):8, 2024. doi: 10. 1007/S44212-024-00042-Y.

- Yanjie Fu, Pengyang Wang, Jiadi Du, Le Wu, and Xiaolin Li. Efficient region embedding with multi-view spatial networks: A perspective of locality-constrained spatial autocorrelations. In *Proceedings of the 32rd AAAI Conference on Artificial Intelligence*, pp. 906–913, 2019.
- William L. Hamilton, Zhitao Ying, and Jure Leskovec. Inductive representation learning on large graphs. In Isabelle Guyon, Ulrike von Luxburg, Samy Bengio, Hanna M. Wallach, Rob Fergus, S. V. N. Vishwanathan, and Roman Garnett (eds.), *Advances in Neural Information Processing Systems 30: Annual Conference on Neural Information Processing Systems 2017, December 4-9, 2017, Long Beach, CA, USA*, pp. 1024–1034, 2017.
- Kaveh Hassani and Amir Hosein Khas Ahmadi. Contrastive multi-view representation learning on graphs. In *Proceedings of the 37th International Conference on Machine Learning, ICML 2020, 13-18 July 2020, Virtual Event*, volume 119 of *Proceedings of Machine Learning Research*, pp. 4116–4126. PMLR, 2020.
- Weiming Huang, Daokun Zhang, Gengchen Mai, Xu Guo, and Lizhen Cui. Learning urban region representations with pois and hierarchical graph infomax. *ISPRS Journal of Photogrammetry and Remote Sensing*, 196:134–145, 2023. ISSN 0924-2716. doi: https://doi.org/10.1016/j.isprsjprs. 2022.11.021.
- Bo Hui, Da Yan, Wei-Shinn Ku, and Wenlu Wang. Predicting economic growth by region embedding: A multigraph convolutional network approach. In Mathieu d'Aquin, Stefan Dietze, Claudia Hauff, Edward Curry, and Philippe Cudré-Mauroux (eds.), CIKM '20: The 29th ACM International Conference on Information and Knowledge Management, Virtual Event, Ireland, October 19-23, 2020, pp. 555–564. ACM, 2020. doi: 10.1145/3340531.3411882.
- Porter Jenkins, Ahmad Farag, Suhang Wang, and Zhenhui Li. Unsupervised representation learning of spatial data via multimodal embedding. In Wenwu Zhu, Dacheng Tao, Xueqi Cheng, Peng Cui, Elke A. Rundensteiner, David Carmel, Qi He, and Jeffrey Xu Yu (eds.), *Proceedings of the 28th ACM International Conference on Information and Knowledge Management, CIKM 2019, Beijing, China, November 3-7, 2019*, pp. 1993–2002. ACM, 2019. doi: 10.1145/3357384.3358001.
- Sina Keller, Raoul Gabriel, and Johanna Guth. Machine learning framework for the estimation of average speed in rural road networks with openstreetmap data. *ISPRS Int. J. Geo Inf.*, 9(11):638, 2020. doi: 10.3390/IJGI9110638.
- Yi Li, Weiming Huang, Gao Cong, Hao Wang, and Zheng Wang. Urban region representation learning with openstreetmap building footprints. In Ambuj K. Singh, Yizhou Sun, Leman Akoglu, Dimitrios Gunopulos, Xifeng Yan, Ravi Kumar, Fatma Ozcan, and Jieping Ye (eds.), *Proceedings of the 29th ACM SIGKDD Conference on Knowledge Discovery and Data Mining, KDD 2023, Long Beach, CA, USA, August 6-10, 2023*, pp. 1363–1373. ACM, 2023. doi: 10.1145/3580305. 3599538.
- Rohin Manvi, Samar Khanna, Gengchen Mai, Marshall Burke, David B. Lobell, and Stefano Ermon. Geollm: Extracting geospatial knowledge from large language models. In *The Twelfth International Conference on Learning Representations, ICLR 2024, Vienna, Austria, May 7-11, 2024*. OpenReview.net, 2024.
- William B. Meyer and B. L. Turner. Human population growth and global land-use/cover change. *Annual Review of Ecology and Systematics*, 23:39–61, 1992. ISSN 00664162.
- Nikhil Naik, Jade Philipoom, Ramesh Raskar, and César Hidalgo. Streetscore predicting the perceived safety of one million streetscapes. In *Proceedings of the 2014 IEEE Conference on Computer Vision and Pattern Recognition*, pp. 793–799, 2014.
- Arvind Neelakantan, Tao Xu, Raul Puri, Alec Radford, Jesse Michael Han, Jerry Tworek, Qiming Yuan, Nikolas Tezak, Jong Wook Kim, Chris Hallacy, Johannes Heidecke, Pranav Shyam, Boris Power, Tyna Eloundou Nekoul, Girish Sastry, Gretchen Krueger, David Schnurr, Felipe Petroski Such, Kenny Hsu, Madeleine Thompson, Tabarak Khan, Toki Sherbakov, Joanne Jang, Peter Welinder, and Lilian Weng. Text and code embeddings by contrastive pre-training. *CoRR*, abs/2201.10005, 2022.

- Yansong Ning and Hao Liu. Urbankgent: A unified large language model agent framework for urban knowledge graph construction, 2024.
 - Manish Prajapat, Mojmir Mutny, Melanie N. Zeilinger, and Andreas Krause. Submodular reinforcement learning, 2024.
 - Srinivas S. Pulugurtha, Venkata Ramana Duddu, and Yashaswi Kotagiri. Traffic analysis zone level crash estimation models based on land use characteristics. *Accident Analysis & Prevention*, 50: 678–687, 2013. ISSN 0001-4575.
 - Stephen E. Robertson and Steve Walker. Some simple effective approximations to the 2-poisson model for probabilistic weighted retrieval. In W. Bruce Croft and C. J. van Rijsbergen (eds.), *Proceedings of the 17th Annual International ACM-SIGIR Conference on Research and Development in Information Retrieval. Dublin, Ireland, 3-6 July 1994 (Special Issue of the SIGIR Forum)*, pp. 232–241. ACM/Springer, 1994. doi: 10.1007/978-1-4471-2099-5_24.
 - John Schulman, Filip Wolski, Prafulla Dhariwal, Alec Radford, and Oleg Klimov. Proximal policy optimization algorithms, 2017.
 - Toru Shimizu, Takahiro Yabe, and Kota Tsubouchi. Improving land use classification using human mobility-based hierarchical place embeddings. In 19th IEEE International Conference on Pervasive Computing and Communications Workshops and other Affiliated Events, Per-Com Workshops 2021, Kassel, Germany, March 22-26, 2021, pp. 305–311. IEEE, 2021. doi: 10.1109/PERCOMWORKSHOPS51409.2021.9431083.
 - Hongjian Wang and Zhenhui Li. Region representation learning via mobility flow. In Ee-Peng Lim, Marianne Winslett, Mark Sanderson, Ada Wai-Chee Fu, Jimeng Sun, J. Shane Culpepper, Eric Lo, Joyce C. Ho, Debora Donato, Rakesh Agrawal, Yu Zheng, Carlos Castillo, Aixin Sun, Vincent S. Tseng, and Chenliang Li (eds.), Proceedings of the 2017 ACM on Conference on Information and Knowledge Management, CIKM 2017, Singapore, November 06 10, 2017, pp. 237–246. ACM, 2017. doi: 10.1145/3132847.3133006.
 - Zhecheng Wang, Haoyuan Li, and Ram Rajagopal. Urban2vec: Incorporating street view imagery and pois for multi-modal urban neighborhood embedding. In *The Thirty-Fourth AAAI Conference on Artificial Intelligence, AAAI 2020, The Thirty-Second Innovative Applications of Artificial Intelligence Conference, IAAI 2020, The Tenth AAAI Symposium on Educational Advances in Artificial Intelligence, EAAI 2020, New York, NY, USA, February 7-12, 2020*, pp. 1013–1020. AAAI Press, 2020. doi: 10.1609/AAAI.V34I01.5450.
 - Shangbin Wu, Xu Yan, Xiaoliang Fan, Shirui Pan, Shichao Zhu, Chuanpan Zheng, Ming Cheng, and Cheng Wang. Multi-graph fusion networks for urban region embedding. In Luc De Raedt (ed.), *Proceedings of the Thirty-First International Joint Conference on Artificial Intelligence, IJCAI* 2022, Vienna, Austria, 23-29 July 2022, pp. 2312–2318. ijcai.org, 2022. doi: 10.24963/IJCAI. 2022/321.
 - Yanxin Xi, Tong Li, Huandong Wang, Yong Li, Sasu Tarkoma, and Pan Hui. Beyond the first law of geography: Learning representations of satellite imagery by leveraging point-of-interests. In Frédérique Laforest, Raphaël Troncy, Elena Simperl, Deepak Agarwal, Aristides Gionis, Ivan Herman, and Lionel Médini (eds.), WWW '22: The ACM Web Conference 2022, Virtual Event, Lyon, France, April 25 29, 2022, pp. 3308–3316. ACM, 2022. doi: 10.1145/3485447.3512149.
 - Yibo Yan, Haomin Wen, Siru Zhong, Wei Chen, Haodong Chen, Qingsong Wen, Roger Zimmermann, and Yuxuan Liang. Urbanclip: Learning text-enhanced urban region profiling with contrastive language-image pretraining from the web. In Tat-Seng Chua, Chong-Wah Ngo, Ravi Kumar, Hady W. Lauw, and Roy Ka-Wei Lee (eds.), *Proceedings of the ACM on Web Conference 2024, WWW 2024, Singapore, May 13-17, 2024*, pp. 4006–4017. ACM, 2024. doi: 10.1145/3589334.3645378.
 - Zijun Yao, Yanjie Fu, Bin Liu, Wangsu Hu, and Hui Xiong. Representing urban functions through zone embedding with human mobility patterns. In Jérôme Lang (ed.), *Proceedings of the Twenty-Seventh International Joint Conference on Artificial Intelligence, IJCAI 2018, July 13-19, 2018, Stockholm, Sweden*, pp. 3919–3925. ijcai.org, 2018. doi: 10.24963/IJCAI.2018/545.

- Jing Yuan, Yu Zheng, and Xing Xie. Discovering regions of different functions in a city using human mobility and pois. In Qiang Yang, Deepak Agarwal, and Jian Pei (eds.), *The 18th ACM SIGKDD International Conference on Knowledge Discovery and Data Mining, KDD '12, Beijing, China, August 12-16, 2012*, pp. 186–194. ACM, 2012. doi: 10.1145/2339530.2339561.
- Chao Zhang, Keyang Zhang, Quan Yuan, Haoruo Peng, Yu Zheng, Tim Hanratty, Shaowen Wang, and Jiawei Han. Regions, periods, activities: Uncovering urban dynamics via cross-modal representation learning. In Rick Barrett, Rick Cummings, Eugene Agichtein, and Evgeniy Gabrilovich (eds.), *Proceedings of the 26th International Conference on World Wide Web, WWW 2017, Perth, Australia, April 3-7, 2017*, pp. 361–370. ACM, 2017a. doi: 10.1145/3038912.3052601.
- Liang Zhang, Cheng Long, and Gao Cong. Region embedding with intra and inter-view contrastive learning. *CoRR*, abs/2211.08975, 2022. doi: 10.48550/ARXIV.2211.08975.
- Mingyang Zhang, Tong Li, Yong Li, and Pan Hui. Multi-view joint graph representation learning for urban region embedding. In Christian Bessiere (ed.), *Proceedings of the Twenty-Ninth International Joint Conference on Artificial Intelligence, IJCAI 2020*, pp. 4431–4437. ijcai.org, 2020. doi: 10.24963/IJCAI.2020/611.
- Xiuyuan Zhang, Shihong Du, and Qiao Wang. Hierarchical semantic cognition for urban functional zones with vhr satellite images and poi data. *ISPRS Journal of Photogrammetry and Remote Sensing*, 132:170–184, 2017b. ISSN 0924-2716.
- Yunchao Zhang, Yanjie Fu, Pengyang Wang, Xiaolin Li, and Yu Zheng. Unifying inter-region autocorrelation and intra-region structures for spatial embedding via collective adversarial learning. In Ankur Teredesai, Vipin Kumar, Ying Li, Rómer Rosales, Evimaria Terzi, and George Karypis (eds.), Proceedings of the 25th ACM SIGKDD International Conference on Knowledge Discovery & Data Mining, KDD 2019, Anchorage, AK, USA, August 4-8, 2019, pp. 1700–1708. ACM, 2019. doi: 10.1145/3292500.3330972.
- Wenting Zhao, Gongping Xu, Zhen Cui, Siqiang Luo, Cheng Long, and Tong Zhang. Deep graph structural infomax. In Brian Williams, Yiling Chen, and Jennifer Neville (eds.), *Thirty-Seventh AAAI Conference on Artificial Intelligence, AAAI 2023, Thirty-Fifth Conference on Innovative Applications of Artificial Intelligence, IAAI 2023, Thirteenth Symposium on Educational Advances in Artificial Intelligence, EAAI 2023, Washington, DC, USA, February 7-14, 2023*, pp. 4920–4928. AAAI Press, 2023. doi: 10.1609/AAAI.V37I4.25618.
- Yu Zheng, Furui Liu, and Hsun-Ping Hsieh. U-air: when urban air quality inference meets big data. In Inderjit S. Dhillon, Yehuda Koren, Rayid Ghani, Ted E. Senator, Paul Bradley, Rajesh Parekh, Jingrui He, Robert L. Grossman, and Ramasamy Uthurusamy (eds.), *The 19th ACM SIGKDD International Conference on Knowledge Discovery and Data Mining, KDD 2013, Chicago, IL, USA, August 11-14, 2013*, pp. 1436–1444. ACM, 2013. doi: 10.1145/2487575.2488188.

A DATA SOURCE

 In this paper, all datasets we used are available online. We hereby provide their links in Table 5.

Table 5: Data sources and links

Data Type	Source	Link
POI datasets - Bejing, Shanghai	Gaode - API search	https://lbs.amap.com/
POI datasets - Singapore, NYC	OpenStreetMap	https://download.geofabrik.de/
Region partitions - Beijing, Shanghai	GADM	https://gadm.org
Region partitions - Singapore	OpenStreetMap	OSM Overpass API
Region partitions - NYC	NYC Planning	https://www.nyc.gov/content/planning/pages/
Population density	WorldPop	https://hub.worldpop.org
House prices	Beike	https://ke.com
Gross Domestic Product (GDP)	RESDP	https://doi.org/10.12078/2017121102

B IMPLEMENTATION DETAILS

Due to the original settings of different baselines, the dimension d of generated representation varies. The dimension d=768 for BERT and SpaBERT, d=1536 for OpenAI, d=64 for HGI, d=512 for DGI and MVGRL, d=1024 for CityFM and GraphSAGE. For our SubUrban, the average pooling of hypernode subset results in the same output dimension d=768 as the BERT embeddings of POIs in regions. We set 15 rounds of CEM optimization with early stopping, 10 rounds of RL expansion for both training and testing phases of SubUrban, with a training set comprising only 1/10 of regions that provide downstream feedback. All experiments are conducted on 1 NVIDIA V100 32 GB GPU unit.

C LLM Instructions

C.1 LLM Instructions on POI Pre-Selection

To prepare the POI set for the start point of SubUrban, which is also the POI preprocessing step with LLM knowledge mentioned in Section 4.1, we generated representative keywords for each urban region using GPT4. In the case of New York City, the five Boroughs (*Manhattan*, *Brooklyn*, *Queens*, *Bronx*, *Staten Island*) are used as region units.

Prompt Template. We use GPT to produce exactly 10 representative keywords for each Borough in NYC. The user prompt specified categories such as landmarks, shopping centers, transportation hubs, cultural venues, residential or neighborhood features, businesses, historical sites, and major districts. The template of the prompt is as follows:

```
Generate exactly 10 representative keywords for each Borough: {areas}

BOROUGH_NAME_1: keyword1, keyword2, keyword3, keyword4, keyword5, keyword6, keyword7, keyword8, keyword9, keyword10

BOROUGH_NAME_2: keyword1, keyword2, keyword3, keyword4, keyword5, keyword6, keyword7, keyword8, keyword9, keyword10
```

Output Format. The final output for each Borough was stored in a tab-separated format as follows:

```
BOROUGH_NAME 'keyword1','keyword2',...,'keyword10'
```

C.2 LLM Instructions on CEM

As mentioned in Section 4.3, we use LLM to instruct the CEM process for a faster convergence of the optimal category weights searching process. We use DeepSeek-R1 here for instruction since it takes much lower costs through frequent querying compared to the GPT series of LLMs. The details of the CEM contents prompted by DeepSeek-R1 are listed in Table 6, and the details of the LLM responses split as adjustments back to the CEM process are listed in Table 7.

Table 6: CEM contents prompted to LLM

Content	Expression	Description						
Short-term summary								
Recent best mixed rewards Current distribution parameters Elite sample statistics	$ \begin{cases} R_{\text{best}}^{(t-2)}, R_{\text{best}}^{(t-1)}, R_{\text{best}}^{(t)} \} \\ \boldsymbol{\mu}^{(t)}, \boldsymbol{\sigma}^{(t)} \\ \boldsymbol{\mu}_{\text{elit}}^{(t)}, \boldsymbol{\sigma}_{\text{elite}}^{(t)} \\ \Delta R_{\text{best}}^{(t)}, \Delta^2 R_{\text{best}}^{(t)} \\ \Delta r_{\text{ank}}^{(t)} = 1 - \tau \left(r^{(t)}, r^{(t-1)} \right) \\ \text{Stability}^{(t)} = \frac{1}{1 + \text{Var}\{R_{\text{best}}^{(t-k+1)} - R_{\text{best}}^{(t-k)}\}} \\ \rho_i^{(t)} = \text{corr} \left(w_i^{(t,j)} - \boldsymbol{\mu}_i^{(t)}, R_{\text{mix}}^{(t,j)} \right) $	Best mixed reward over the last three iterations. Sampling means and stds for category weights. Mean and std of top-performing samples.						
Performance trends Ranking drift Stability indicator	$\Delta R_{\text{best}}^{(\tau)}, \Delta^2 R_{\text{best}}^{(\tau)}$ $\Delta_{\text{rank}}^{(t)} = 1 - \tau(r^{(t)}, r^{(t-1)})$ $\text{Stability}^{(t)} = \frac{1}{1 + V_{\text{col}} R_{\text{col}}^{(t-k+1)} R_{\text{col}}^{(t-k)}}$	First and second differences of the best reward. Change in weight ranking (Kendall's τ). Inverse variance of recent reward changes.						
Category–reward correlations	$\rho_i^{(t)} = \operatorname{corr}(w_i^{(t,j)} - \mu_i^{(t)}, R_{\operatorname{mix}}^{(t,j)})$	Correlation between weight deviations and reward.						
	Long-term history							
Historic record	$\{(\mu^{(\tau)}, \sigma^{(\tau)}, \operatorname{adj}^{(\tau)}, R_{\operatorname{best}}^{(\tau)})\}_{\tau=1}^{t-1}$	Past μ , σ , adjustments, and best rewards.						

Table 7: LLM instruction contents to CEM

Adjustment Content	Field / Symbol	Description
Per-category mean shift	$\Delta \mu_i$	Additive change applied to μ_i
Per-category std shift	$\Delta\sigma_i$	Additive change applied to σ_i
Restart distribution	$restart_i$	Reinitialize $\mu_i \sim \mathcal{U}(0.8, 1.2), \sigma_i \sim \mathcal{U}(0.4, 0.6)$
Smoothing factor update	α	New interpolation weight between old and elite statistics
Elite fraction update	$f_{ m elite}$	New fraction of samples selected as elite

D ADDITIONAL CONTENTS OF EXPERIMENTS

D.1 BASELINES

(1) Baselines

- BERT (Devlin et al., 2019b): BERT is a representative pre-trained language model that excels in capturing deep semantics. We use it to encode POIs and average for the region embedding.
- OpenAI (Neelakantan et al., 2022): OpenAI text-embedding-3-small provides high-quality text embeddings trained with large-scale contrastive objectives. We adopt it to encode POIs and aggregate for region embedding by average pooling.
- GraphSage (Hamilton et al., 2017): This classical graph learning algorithm samples and aggregates neighbor nodes to compute node embeddings. It is commonly used as a geospatial representation learning baseline with node feature or graph structure reconstruction objectives.
- DGI (Zhao et al., 2023): This method maximizes the mutual information between node and graph embeddings. We take its graph embedding as the region representation. It doesn't explicitly learn geospatial correlations.
- MVGRL (Hassani & Ahmadi, 2020): Inspired by DGI, this method maximizes the mutual information between the node and graph embedding from the original graph and an augmented graph constructed by graph diffusion. We use its graph embedding as the region representation. It doesn't explicitly learn geospatial correlations.

- HGI (Huang et al., 2023): Inspired by DGI, this method incorporates geospatial domain knowledge by hierarchically maximizing the mutual information between POI, region, and city representations. It proposes a novel rule-based strategy of positive and negative sampling to preserve fine-grained and holistic information simultaneously.
- CityFM (Balsebre et al., 2024): This method learns general-purpose geospatial representations from multimodal OpenStreetMap node, polyline, and polygon data. We use its node encoder to encode POI representations and average them as the region representation.

(2) Model variants

- SubUrban w/o RL: This is a variant of our model where we remove the proposed RL training process mentioned in Section 4.2 and use random selection instead.
- SubUrban w/o CEM: This is also a variant of our model where we remove the proposed LLM-instruct CEM optimization mentioned in Section 4.3.

D.2 CROSS-TASK PERFORMANCE IN SHANGHAI

We also conduct the cross-task experiments in Shanghai. SubUrban still holds the superior performance of all tasks compared to all of the baseline methods shown in Table 8.

Table 8: Population Density, House Price, and GDP Density Prediction in Shanghai

Models	Population			House Price			GDP Density		
	MAE↓	RMSE↓	$R^2\uparrow$	MAE↓	RMSE↓	$R^2\uparrow$	MAE↓	RMSE↓	$R^2\uparrow$
DEDE A	9375.19	14235.93	0.47	15244.90	21849.39	0.35	1461.75	2478.55	0.60
BERT-Avg	(± 75.37)	(± 203.54)	(± 0.01)	(± 799.72)	(± 1665.11)	(± 0.08)	(± 70.10)	(± 186.95)	(± 0.04)
O AT A	9816.80	14579.09	0.44	15566.60	22078.45	0.35	1601.76	2644.08	0.55
OpenAI-Avg	(± 108.09)	(± 305.37)	(± 0.02)	(± 446.11)	(± 1158.55)	(± 0.03)	(± 72.66)	(± 196.10)	(± 0.02)
GraphSage	8759.62	13682.10	0.53	15348.31	23770.38	0.45	1454.01	2515.51	0.59
	(± 388.16)	(± 644.79)	(± 0.02)	(± 804.33)	(± 3416.98)	(± 0.07)	(± 74.77)	(± 233.19)	(± 0.04)
DGI	9315.73	14110.26	0.47	15806.18	23471.61	0.36	1536.07	2551.83	0.60
DGI	(± 441.15)	(± 1157.06)	(± 0.05)	(± 1539.58)	(± 4101.79)	(± 0.09)	(± 49.22)	(± 125.26)	(± 0.03)
MVGRL	9087.51	13646.88	0.49	16290.52	24811.52	0.36	1775.15	2904.99	0.48
MVGKL	(± 573.17)	(± 1078.60)	(± 0.06)	(± 923.21)	(± 2817.58)	(± 0.05)	(± 31.41)	(± 142.52)	(± 0.04)
HGI	7464.74	11642.35	0.66	15443.26	24436.62	0.42	1199.68	2247.50	0.67
поі	(± 182.11)	(± 289.60)	(± 0.02)	(± 1043.29)	(± 3630.39)	(± 0.08)	(± 68.44)	(± 126.82)	(± 0.02)
CityEM	6558.20	10677.55	0.71	14160.05	21092.11	0.43	867.13	1606.45	0.83
CityFM	(± 108.37)	(± 218.36)	(± 0.01)	(± 692.90)	(± 1529.19)	(± 0.06)	(± 52.74)	(± 122.13)	(± 0.02)
SubUrban	5684.80	9673.78	0.75	13801.49	20511.39	0.47	821.56	1507.51	0.84
SubUrban	(± 356.93)	(± 716.99)	(± 0.02)	(± 1327.04)	(± 4684.24)	(± 0.06)	(± 55.52)	(± 87.78)	(± 0.02)

D.3 ABLATION STUDY OF LLM INTERVENTION

LLM intervents in two parts of SubUrban. The first part is preprocessing POI for cold-starting candidate subsets mentioned in Section 4.1, and the second part is instructing CEM optimization for attention weights of different POI categories mentioned in Section 4.3. The ablation studies of these LLM parts are based on two experiments:

We evaluate the POI subsets preprocessed by LLM through the RL training rounds comparison between LLM subsets and randomly sampled subsets as inputs. The results in Figure 5 show that LLM-processed subsets converge to higher mixed rewards compared to randomly sampled subsets during training rounds, especially the consistent surpass during training in Shanghai, which validates the effectiveness of keeping intra-region features by LLM for training a better hypernode expansion model incorporating complementary inter-region relations.

And we evaluate the LLM-instructed CEM optimization with the basic CEM optimization without LLM instructions. As illustrated in Figure 6, the LLM instruction accelerates the convergence of CEM optimization for the best attention weights for POI categories in both Beijing and Shanghai, which validates the power of directing CEM optimization by LLM.



Figure 5: RL Training Rounds comparison between LLM Processed POIs input and Randomly Sampled POIs input.

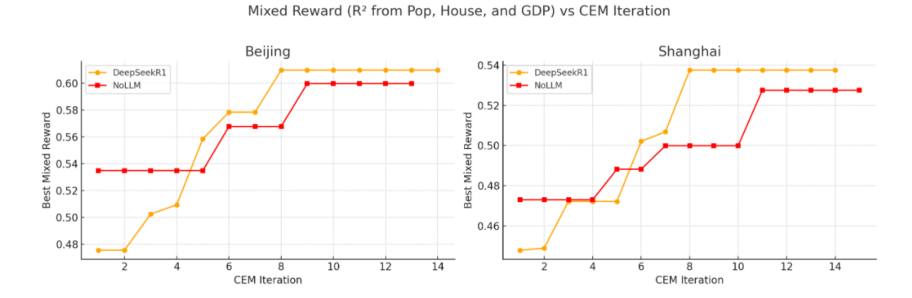


Figure 6: CEM iterations comparison between DeepSeek-R1 instructed and nollm-instruct.

D.4 PARAMETER SENSITIVITY ANALYSIS

We evaluate the parameter sensitivity of SubUrban on two hyperparameters, which are the penalty coefficient α and Top-K in each round of expansion for each region. The penalty coefficient α in the Buffer Controller (Eq. 9) controls how strongly buffer expansion is penalized during RL training, while the Top-K parameter in the two-stage policy network (Section 4.2.2) determines how many POI candidates are extended per round. The details of the sensitivity results are shown in Figure 7.

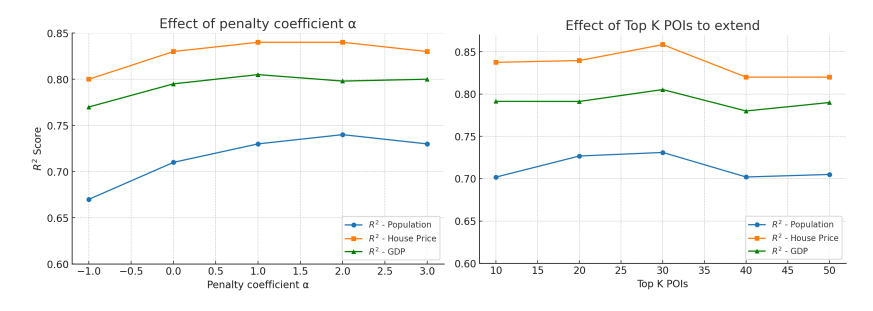


Figure 7: Parameter sensitivity analysis: (Left) Effect of penalty coefficient α in Buffer Controller; (Right) Effect of Top K POIs to extend on R² for population and house price prediction in Beijing.

D.5 ANALYSIS OF A CASE REGION WITH EXPANSION

We randomly select a region (ID:111) in Beijing with a high population density as our observation target. We compare the Original Region, Random Expansion, SubUrban expansion with population task reward as feedback only (SubUrban_Pop), and SubUrban with the combined reward of triple tasks as feedback (SubUrban_Triple). The average buffer distance after 10 rounds of expansion is around 3 kilometers for each region in Beijing.

 From the spatial aspect, visualizations are shown in Figure 8. Each figure illustrates the spatial distributions of POIs after 10 rounds of expansion. Different colors represent the categories of extended POIs around this region. Compared to the Random Expansion, the spatial distribution of expanded POIs are more evenly distributed in geographical space with a few clusters, which proves that the RL-trained model ensures a less biased and spatially balanced exploration space due to the coverage restriction in the definition of the state.

From the semantic aspect, statistics of POIs categories after expansion are shown in Figure 9. The grey bars in the histogram represent the original distribution of POI categories, blue bars represent the LLM preselected POI categories, while orange bars represent the expanded categories of POIs. Firstly, based on the pre-trained and retrieved knowledge for this region, LLM distinguishes that categories such as "Address", "Companies", and "Government" are especially relevant to the functionality of this region, so that it keeps these POIs more than others. Secondly, SubUrban variants further focus on a smaller set of categories compared with Random Expansion, suggesting a tendency to concentrate on task-relevant semantics rather than aimless diversification. Thirdly, SubUrban_Pop expands more "Shopping" POIs, which is intuitively consistent with the strong connection between shopping activities and population density, while SubUrban_Triple shifts toward "Public" and "CarSales" categories, reflecting additional relevance to GDP and housing price prediction.

In summary, these spatial and semantic results confirm that SubUrban does not expand POIs arbitrarily, but instead learns to autonomously balance spatial coverage, semantic focus, and task-specific relevance in a way that is both interpretable and practically meaningful.

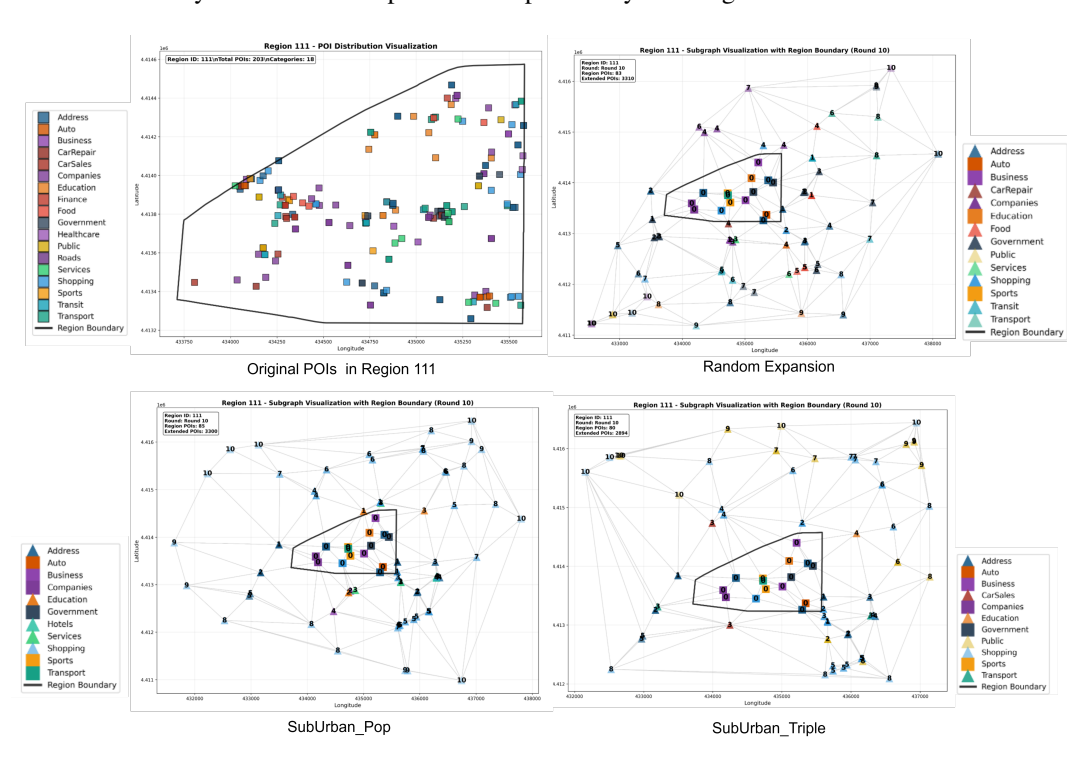


Figure 8: Visualizations of Original vs. Random Expansion vs. SubUrban_Triple vs. SubUrban_Pop.

E DISCLOSURE OF LLM USAGE

We made limited use of GPT-5 for editing purposes, specifically to enhance clarity and grammar of the text. All core aspects of this research, including idea formulation, experimental methodology, and result interpretation, were conducted without LLM assistance.

Statistics of POI categories in Region 111 in Beijing ---- Original (if lower than Initial+Expansion) Original Initial Expansion SubUrban_triple Expansion SubUrban_pop Expansion Random_Expand Expansion Roads Healthcare Finance Sports CarSales Food Public CarRepair Services Auto Business Transit Education Shopping Government Transport Companies Address 20 30 Number of POIs 20 30 Number of POIs 20 30 Number of POIs

Figure 9: Statistics of expanded POI categories from SubUrban_Triple vs. SubUrban_Pop vs. Random Expansion.